A NUMERICAL STUDY OF SUPERCONVERGENCE OF THE DISCONTINUOUS GALERKIN METHOD BY PATCH RECONSTRUCTION

ZEXUAN LIU, ZHIYUAN SUN, AND JERRY ZHIJIAN YANG

Abstract. We numerically investigate the superconvergence property of the discontinuous Galerkin method by patch reconstruction. The convergence rate $2m + 1$ can be observed at the grid points and barycenters in one dimensional case with uniform partitions. The convergence rate $m + 2$ is achieved at the center of the element face in two and three dimensions. The meshes are uniformly partitioned into triangles/tetrahedrons or squares/hexahedrons. We also demonstrate the details of the implementation of the proposed method. The numerical results for all three dimensional cases are presented to illustrate the proposition.

keyword: superconvergence, discontinuous Galerkin method, patch reconstruction
MSC2010: 49N45; 65N21

1. Introduction

The discontinuous Galerkin method by patch reconstruction(PRDG) was firstly introduced in [12] by Li et al. to solve elliptic equations. The method has been successfully applied into the biharmonic problem [11], the Stokes problem [13, 14], the eigenvalue problem [15], the linear elasticity problem [16], the convection-diffusion problem [18] and the sequential least square method [17]. This method's original idea is motivated by the patch reconstruction technique in the finite volume scheme for the hydrodynamic solver [19]. Benefiting from the least square patch reconstruction, a novel piecewise polynomial discontinuous finite element space is constructed. The space is a subspace of the general discontinuous Galerkin(DG) space, which enables the method to enjoy the well-developed theories and schemes for the DG method. The propose of this article is to introduce the implementation and investigate the superconvergence property numerically of the PRDG method.

Superconvergence properties of the finite element method are classical topics which have been well studied by many [10, 3, 20]. The properties can be employed to design the *a posterior* estimator for h-refinement [1] and the post-processing strategies [24]. In the last decades, there are numerous works focusing on the superconvergence behavior of the DG method [6, 9, 8, 23, 4]. In particular, Cockburn et al. [7] studied the superconvergence of the LDG method for elliptic equations on the Cartesian grid. Castillo analyzed the superconvergence properties for the DG method with conservative numerical flux in [5]. The weak Galerkin(WG) method was introduced by Wang and Ye in [21], and also observed a superconvergence properties numerically. In [22], Wang et al. analyzed the superconvergence for the polynomial preserving recovered gradient of the WG method.

In this article, we perform a numerical study of the superconvergence of the PRDG method and present the detailed algorithms. The PRDG method only takes one degree of freedom (DOF) per element and achieves arbitrary order with an identical number of unknowns. The method utilizes the DOFs with very high efficiency. In some particular cases, the method even can attain higher accuracy than FEMs with the same quantity of unknowns. The superconvergence property of the PRDG method is also conducive to efficiency, which means the method can attain a desirable digit precision with only a few DOFs. The other advantage of the PRDG method is that it has great flexibility in mesh generation, especially that the polygonal mesh is allowed. However, we only consider the uniform meshes in this paper for the purpose of superconvergence.

The article is organized as follows. The approximation space and the details of the algorithm are introduced in Section 2. We first describe the principle to choose the element patches and the sampling nodes, and then elaborate the process to calculate the global stiff-matrix. Section 3 states the approximation properties of such space and the superconvergence properties of the proposed method. Numerical experiments are presented in Section 4 to demonstrate the properties of the resulting linear system and to verify the theoretical results in all 3 dimensions.

2. Numerical Implementation of the Discontinuous Galerkin Method by Patch Reconstruction

We consider an open bounded Lipschitz domain Ω in $\mathbb{R}^D$,$D = 1, 2, 3$, such as a convex polygonal domain in $\mathbb{R}^D$. Let $\mathcal{T}_h$ be a uniform partition of domain Ω. Let h_K and $|K|$ denote its diameter and area/volume, respectively. With the uniform partition, $h\colon = h_K$. The arbitrary polygonal/polyhedron mesh is allowed in this method. However, we focus our discussion on uniform meshes for the purpose of the superconvergence investigation. The shape regularity constraints will be claimed in the next section, and we just focus on the numerical implementation here.

2.1. **Reconstruction and Interpolation.**

With qualified partitions $\mathcal{T}_h$, we expect to define a finite element space V_h and an interpolation operator $\mathcal{R}$ on the mesh at a reasonable cost. If the high order polynomial approximation is needed, a common approach is to define the numerous DOFs locally on each element. To avoid abusing the DOFs, we define only one DOF per element. It is denoted with x_K for the sampling node. Let U_h be the piecewise constant space associated with $\mathcal{T}_h$, i.e.,

$$U_h\colon = \{\, v \in L^2(\Omega) \;|\; v|_K \in \mathbb{P}^0(K)\}.$$

Now we construct the finite element space V_h by the space U_h. More precisely, the finite element space with piecewise polynomials V_h can be regarded as the U_h embedded by the reconstruction operator $\mathcal{R}$, which can be expressed as follows,

$$V_h := \mathcal{R}(U_h).$$

Since there is only one DOF per element and it requires more DOFs to construct higher order polynomial, the patch reconstruction technique is used. The high order polynomial is constructed from the element patch $S(K)$. $S(K)$ is a subset of $\mathcal{T}_h$ that includes K itself and the other elements around K. The sampling node x_K is assigned for each element K, which is a point located inside the element. The details of how to set up the sampling nodes and the element patch will be discussed later. $\mathcal{I}_K$ denotes the set of sampling nodes corresponding to $S(K)$. Let $\#\mathcal{I}_K$ denote the number of elements belonging to $\mathcal{I}_K$, and $\#S(K)$ denotes the number of elements belonging to $S(K)$.

Now we introduce how to obtain the local approximation polynomial with the sampling nodes and the element patch. For $\forall v \in U_h$ and $\forall K \in \mathcal{T}_h$, a local polynomial $\mathcal{R}_K v$ of degree m can be found by seeking the best discrete local least-squares approximation.

$$\mathcal{R}_K v = \arg \min_{p \in \mathbb{P}^m(S(K))} \sum_{x \in \mathcal{I}_K} |v(x) - p(x)|^2 . \tag{2.1}$$

$\mathcal{R}_K v$ gives an interpolation polynomial on the patch $S(K)$. We limit the interpolation on element K. The global interpolation operator $\mathcal{R}$ is given by

$$(\mathcal{R}v)|_K := (\mathcal{R}_K v)|_K, \quad \forall K \in \mathcal{T}_h.$$

Above is the general process to construct the finite element space V_h, and some points should be clarified here. Firstly, the barycenter of element K is preferred as the sampling node x_K when we investigate the superconvergence of the PRDG method, although it can be chosen inside K. Then, we discuss how to determine the element patch $S(K)$. The number $\#S(K)$ should be larger than the DOFs that the polynomial of degree m needs. The number is

$$m + 1 (D = 1), \quad \frac{m^2 + 3m + 2}{2} (D = 2), \quad \frac{3m^2 + 3m + 2}{2} (D = 3),$$

where D is the dimension of space. A threshold value c_0 is assigned to $\#S(K)$, which is reached $S(K)$ recursively by adding the nearest Von Neumann neighbors. The recursive process is terminated when the size of $S(K)$ meets the requirement. Figure 2.1 demonstrate the appropriate patch with proper regularity and the inappropriate patch with an isolated element. The regularity of the element patch might influence the approximation convergence result. This illustrates the reason why we use the above principle to choose the element patch.

The least square problem (2.1) can be easily solved by the generalized inverse of matrix $M = (A^T A)^{-1} A^T$, where A is the Vandermonde-type matrix. The details of 1D examples can be found in [11], 2D in [13] and 3D in [15]. The matrix M_K stores the information of the basis functions whose value is not zero in element K. The matrix M_K only depends on the sampling nodes set $\mathcal{I}_K$ and it is irrelevant to the vector $v \in U_h$. M_K is calculated offline and stored in memory, which is distinct from the FEM and DG methods. The basis function λ_K is the characteristic function corresponding to K. And the basis functions are not explicitly used in the calculation. The interpolation polynomial with order m of the vector $v \in U_h$ is specified as

$$\mathcal{R}_K v = L M_K v_{\mathcal{I}_K}. \tag{2.2}$$

where L is the basis vector of a polynomial with order m. $L = [1, x, x^2, ..., x^m]$ for 1D, $L = [1, x, y, x^2, xy, y^2, ..., y^m]$ for 2D, and $L = [1, x, y, z, x^2, xy, y^2, xz, yz, z^2, ..., z^m]$ for 3D, respectively.

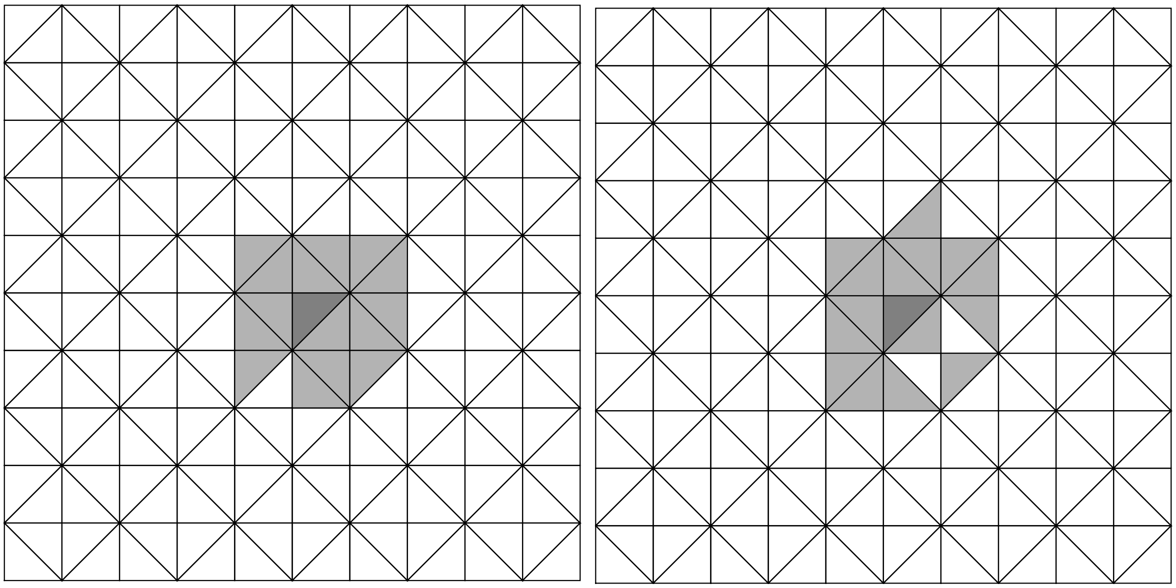

Figure 2.1. The uniform triangle mesh and the appropriate patch(left)/ the inappropriate patch(right).

2.2. **Computation of the stiffness matrix].** We consider the following Poisson problem and solve it with the PRDG method,

$$-\triangle u = f \quad \text{in} \quad \Omega, \qquad u = 0 \quad \text{on} \quad \partial\Omega.$$

Let $\mathcal{E}_h$ denote the collection of all edges of $\mathcal{T}_h$, $\mathcal{E}_h^0$ denote the collection of all the interior edges and $\mathcal{E}_h^b$ denote the collection of all boundary edges. The variational form of the Poisson problem is to seek $u_h \in U_h$ such that

$$a_h(\mathcal{R}u_h, \mathcal{R}v_h) = (f, \mathcal{R}v_h)_h \quad \text{for all} \quad v_h \in U_h. \tag{2.3}$$

The IPDG scheme [2] can be directly applied, where the bilinear term a_h and linear operator $(f, \mathcal{R}v_h)_h$ are defined for any $v_h, w_h \in U_h$ as

$$\begin{aligned} a_h(\mathcal{R}v_h, \mathcal{R}w_h) \colon= &\sum_{K\in\mathcal{T}_h} \int_K \nabla\mathcal{R}v_h \cdot \nabla\mathcal{R}w_h \mathrm{d}x \\ &- \sum_{e\in\mathcal{E}_h} \int_e \left([\![\nabla\mathcal{R}v_h]\!] \{\, \mathcal{R}w_h \,\} + [\![\nabla\mathcal{R}w_h]\!] \{\, \mathcal{R}v_h \,\} \right) \mathrm{d}s \\ &+ \sum_{e\in\mathcal{E}_h} \int_e \frac{\eta}{h_e} [\![\mathcal{R}v_h]\!] \cdot [\![\mathcal{R}w_h]\!] \mathrm{d}s, \end{aligned} \tag{2.4}$$

and

$$(f, \mathcal{R}v_h)_h \colon= \sum_{K\in\mathcal{T}_h} \int_K f\mathcal{R}v_h \mathrm{d}x, \tag{2.5}$$

where η is a positive constant. The average $\{\, v \,\}$ and the jump operator $[\![v]\!]$ is defined as follows. Assume e is a common edge shared by elements K_1 and K_2, and let n_1 and n_2

be the outward unit normal at e of K_1 and K_2, respectively. Given $v_i:=v|_{\partial K_i}$, we define

$$\{v\}=\frac{1}{2}(v_1+v_2),\quad [\![v]\!]=v_1n_1+v_2n_2,\quad \text{on}\ \ e\in\mathcal{E}_h^0.$$

For a vector-valued function φ, we define φ_1 and φ_2 similarly,

$$\{\varphi\}=\frac{1}{2}(\varphi_1+\varphi_2),\quad [\![\varphi]\!]=\varphi_1\cdot n_1+\varphi_2\cdot n_2,\quad \text{on}\ e\in\mathcal{E}_h^0.$$

For $e\in\mathcal{E}_h^b$, let

$$[\![v]\!]=vn,\quad \{\varphi\}=\varphi.$$

The linear algebra system is obtained from the weak form (2.3),

$$Au_h=F, \tag{2.6}$$

where A is the global stiff matrix whose size is $N\times N$, $u_h\in U_h$ is a $N\times 1$ vector, and F is the right hand side(RHS) which also is a $N\times 1$ vector. N is the number of elements in $\mathcal{T}_h$.

We now illuminate the computation of the right hand side F. The $i-$th component of F is the numerical integration of the inner product between f and λ_{K_i}, where λ_{K_i} is the basis function corresponding to the element K_i, i.e.

$$F_i=\int_{K_i}f\lambda_{K_i}\mathrm{d}x,$$

As we mentioned, the basis function λ_{K_i} is not explicitly used in the computation. We calculate the local right hand side ψ_{K_i} element by element, then assemble the local RHS ψ_{K_i} to the global RHS F.

$$\psi_{K_i}=\int_{K_i}fLM_{K_i}\mathrm{d}x.$$

The corresponding relation between ψ_{K_i} and F is determined by s_{K_i}.

Similarly, the elements in the global stiff matrix A is computed from $a_h(\lambda_{K_i},\lambda_{K_j})$. It is not explicitly calculated. Instead, the local element stiff matrix κ_{K_i} and local trace stiff matrix κ_e are calculated per element in $\mathcal{T}_h$ and per edge in $\mathcal{E}_h$, respectively. Assembling the locate stiff matrixes gives A.

The size of the local element stiff matrix is $\#S(K_i)\times\#S(K_i)$, and κ_{K_i} is computed as follows

$$\kappa_{K_i}=\int_{K_i}\left(\nabla_xLM_{K_i}\right)^T\left(\nabla_xLM_{K_i}\right)+\left(\nabla_yLM_{K_i}\right)^T\left(\nabla_yLM_{K_i}\right)+\left(\nabla_zLM_{K_i}\right)^T\left(\nabla_zLM_{K_i}\right)\mathrm{d}x.$$

where ∇_xL is the gradient operator on L, $\nabla_xL=[0,1,0,0,2x,y,0,z,0,0,...,mx^{m-1}]$. The vector ∇_yL and ∇_zL are given in the same way. Because the M_{K_i} is calculated offline, the Jacobian matrix and the affine transformation are no longer needed. Numerical integration is conducted on the real element K_i instead of the reference element. Furthermore, the corresponding matrix is constituted by $s_{K_i}^Ts_{K_i}$.

Consider an interior edge $e\in\mathcal{E}_h^0$, which is shared by elements K_i and K_j. The local trace stiff matrix κ_e is calculated on edge e which is relevant with two element patchs

$S(K_i)$ and $S(K_j)$, and its size is $(\#S(K_i)+\#S(K_j)) \times (\#S(K_i)+\#S(K_j))$. But in practice, the matrix κ_e is decomposed to four submatrix κ_{e_1},κ_{e_2},κ_{e_3},κ_{e_4} for simplicity,

$$\kappa_e = \begin{bmatrix} \kappa_{e_1} & \kappa_{e_2} \\ \kappa_{e_3} & \kappa_{e_4}. \end{bmatrix}$$

The sizes of four submartrices are $\#S(K_i) \times \#S(K_i)$, $\#S(K_i) \times \#S(K_j)$, $\#S(K_j) \times \#S(K_i)$ and $\#S(K_j) \times \#S(K_j)$, respectively. Numerical integration of κ_{e_1} is calculated by

$$\begin{aligned} \kappa_{e_1} = & -\frac{1}{2}\int_e \left(\nabla_x LM_{K_i} n_{x_i} + \nabla_y LM_{K_i} n_{y_i} + \nabla_z LM_{K_i} n_{z_i}\right)^T \left(LM_{K_i}\right) \mathrm{d}s \\ & -\frac{1}{2}\int_e \left(LM_{K_i}\right)^T \left(\nabla_x LM_{K_i} n_{x_i} + \nabla_y LM_{K_i} n_{y_i} + \nabla_z LM_{K_i} n_{z_i}\right) \mathrm{d}s \\ & +\frac{\eta}{h_e}\int_e \left(LM_{K_i}\right)^T \left(LM_{K_i}\right) \mathrm{d}s, \end{aligned}$$

where $n_i = (n_{x_i}, n_{y_i}, n_{z_i})$ is the unit outer norm of K_i on e. The other submatrix and the corresponding relation are computed analogously.

We end this section by some comments about the linear system (2.3). The number of unknowns in u_h always equals to the number of elements N. The scale of stiff matrix A always maintains $N \times N$ regardless of the approximation order m which may vary. The sparsity pattern of A may vary when the size of element patch $S(K)$ varies.

3. Superconvergence Results in Elliptic Problems

In this section, we discuss the convergence property of the PRDG method for the elliptic problems. The mesh partition $\mathcal{T}_h$ is uniformly split in all dimensions in this paper. So it satisfies the shape regularity conditions naturally [12]. For the element patch $S(K)$, we define $d_K := \mathrm{diam} S(K)$ and $d = \max_{K\in\mathcal{T}_h} d_K$. Moreover, we assume the following.

Assumption 1 For $\forall K \in \mathcal{T}_h$, there exist constants C and c that are independent of K, such that $B_c \subset S(K) \subset B_C$ with $C \geq 2c$, and $S(K)$ is star-shaped with respect to B_c, where B_c is a disk with radius c.

The **Assumption 1** is the geometric constraint for the element patch, which is also the reason why we must obey the principle to choose the candidate of element patch. Next, we claim the assumption on the sampling node set.

Assumption 2 For any $K \in \mathcal{T}_h$ and $p \in \mathbb{P}_m(S(K))$,

$$p|_{\mathcal{I}(K)} = 0 \quad \text{implies} \quad p|_{S(K)} \equiv 0. \tag{3.1}$$

This assumption leads to the uniqueness of the least squares problem (2.1), which implies that the number $\#\mathcal{I}_K$ must be larger enough. However, the size of the element patch is a subtle issue. When the element patch is taking too large, the diameter d of $S(K)$ increases and might change the numerical error. There is a quantitative estimate of this assumption,

$$\Lambda(m, \mathcal{I}(K)) < \infty$$

with

$$\Lambda(m, \mathcal{I}(K)) := \max_{p \in \mathbb{P}_m(S(K))} \frac{\| p \|_{L^\infty(S(K))}}{\| p|_{\mathcal{I}(K)} \|_{\ell_\infty}}. \tag{3.2}$$

The constant $\Lambda(m, \mathcal{I}(K))$ is analogous to the Lebesgue constant in the approximation theory. The uniform upper bound of $\Lambda(m, \mathcal{I}(K))$ can be found if the element patch satisfies some constraints, we refer to [12] for the details. Now, we are ready to state the approximation property of the local reconstruction operator,

Lemma 3.1. [12, Lemma 3] *There exists a unique solution to* (2.1) *while* Assumption 2 *holds. Furthermore, $\mathcal{R}_K v$ satisfies*

$$\mathcal{R}_K g = g \quad \text{for all} \quad g \in \mathbb{P}_m(S(K)). \tag{3.3}$$

For any $K \in \mathcal{T}_h$ and $g \in C^0(S(K))$, the stability property holds

$$\| \mathcal{R}_K g \|_{L^\infty(K)} \leq \Lambda(m, \mathcal{I}(K)) \sqrt{\# \mathcal{I}(K)} \| g|_{\mathcal{I}(K)} \|_{\ell_\infty}, \tag{3.4}$$

and the quasi-optimal approximation property is valid

$$\| g - \mathcal{R}_K g \|_{L^\infty(K)} \leq \Lambda_m \inf_{p \in \mathbb{P}_m(S(K))} \| g - p \|_{L^\infty(S(K))}, \tag{3.5}$$

where $\Lambda_m := \max_{K \in \mathcal{T}_h} \{1 + \Lambda(m, \mathcal{I}(K)) \sqrt{\# \mathcal{I}(K)}\}$.

The nearly optimal approximation property naturally exists.

Lemma 3.2. [12, Lemma 4] *If* Assumption 2 *holds, then there exists C that for $u \in C^0(\Omega) \cup H^{m+1}(\Omega)$ such that*

$$\| g - \mathcal{R}_K g \|_{L^2(K)} \leq C \Lambda_m h_K d_K^m \, | g |_{H^{m+1}(S(K))} . \tag{3.6}$$

$$\| \nabla (g - \mathcal{R}_K g) \|_{L^2(K)} \leq C \left(h_K^m + \Lambda_m d_K^m \right) | g |_{H^{m+1}(S(K))} . \tag{3.7}$$

The approximation estimates of the global reconstruction operator are as follows,

Lemma 3.3. [12, Equation (3.4)] *For $u \in H^{m+1}(\Omega)$, together with the Agmon inequality and the local approximation estimates* (3.6) *and* (3.7)*, there exist a positive constant C, such that*

$$\| g - \mathcal{R} g \|_{L^2(\Omega)} \leq C \Lambda_m h d^m \, | g |_{H^{m+1}(\Omega)} . \tag{3.8}$$

$$\| \nabla (g - \mathcal{R} g) \|_{L^2(\Omega)} \leq C \left(h^m + \Lambda_m d^m \right) | g |_{H^{m+1}(\Omega)} . \tag{3.9}$$

3.1. **General Convergence Property.** We now introduce the convergence property of the PRDG method for the elliptic problems. The coercivity and the boundedness of a_h are obvious. For sufficiently large η, there exist α and β such that

$$\begin{aligned} a_h(\mathcal{R} v, \mathcal{R} v) &\geq \alpha \| \mathcal{R} v \|^2, && v \in U_h, \\ |a_h(\mathcal{R} v, \mathcal{R} w)| &\leq \beta \| \mathcal{R} v \| \| \mathcal{R} w \|, && v, w \in U_h \text{ and } v, w \in H^1(\mathcal{T}_h). \end{aligned}$$

where the energy norm is defined as

$$\| v \|^2 = \sum_{K \in \mathcal{T}_h} \| \nabla v \|_{L^2(K)}^2 + \sum_{e \in \mathcal{E}_h} |h_e|^{-1} \, \| [\![v]\!] \|_{L^2(e)}^2 .$$

This immediately gives the existence and the uniqueness of the weak form (2.3). The error estimate for the Poisson problem is given by the following theorem.

Theorem 3.4. [12, Theorem 1] *For $u \in H^{m+1}(\Omega)$ and let u_h be the solution of the Poisson problem and* (2.3)*, respectively. Then there exists a positive constant C, such that*

$$\| u - \mathcal{R}u_h \|_{L^2(\Omega)} \leq C \left(h^{m+1} + \Lambda_m d^{m+1} \right) | u |_{H^{m+1}(\Omega)} \tag{3.10}$$

If **Assumption 1** *holds, then we can simplify*(3.10) *into*

$$\| u - \mathcal{R}u_h \|_{L^2(\Omega)} \leq C h^{m+1} | u |_{H^{m+1}(\Omega)} . \tag{3.11}$$

The above estimates are for the general meshes. If we employ uniform meshes, we can obtain a better convergence rate at the barycenters or the face centers of the mesh.

3.2. **Superconvergence Property.** In one dimensional space, the meshes are equally distributed. Then refine the mesh by split one grid into two identical grid, which guarantees each grid points in the coarse mesh will also be the grid points in the fine mesh, see Figure 3.1.

Figure 3.1. The way to refine the mesh.

A convergence rate $2(m+1)$ can be observed at some special point. In one dimensional case, the grid points and the barycenters of the grid have the superconvergence property. We define two norms for the estimates, which are related to the discrete point values. There are N grid points on the uniform partition $\mathcal{T}_h$, which are the barycenters of elements, denoted by $x_1, ..., x_N$. We define the norm $\| \cdot \|_h$ that depends on the mesh as follows,

$$\| u_h \|_h := \sum_{i=1}^{N} \frac{1}{N} |u_h(x_i)|.$$

Since there are two values on the grid points and the discontinuity, we actually investigate the average $\{ \cdot \}$ at the grid points. Assume there are M grid points on the uniform partition $\mathcal{T}_h$, denote with $x_1, ..., x_M$, norm $\| \! | \cdot | \! \|_h$ is defined as follows,

$$|\!\|\, u_h \,|\!\|_h := \sum_{i=1}^{M} \frac{1}{M} | \{ u_h(x_i) \} |.$$

For one dimensional case, we have the following superconvergence result.

Proposition 3.1. *If the partition $\mathcal{T}_h$ are equally divided, u and u_h are the solution in Theorem 3.4, and additionally $u \in H^{2m+1}(\Omega)$, such that the superconvergence property with $2m+1$ order at the grid points and the barycenters are satisfied, i.e.*

$$\begin{aligned} \| u - \mathcal{R}u_h \|_h &\leq C h^{2m+1} | u |_{H^{2m+1}(\Omega)} , \\ |\!\| u - \mathcal{R}u_h |\!\|_h &\leq C h^{2m+1} | u |_{H^{2m+1}(\Omega)} \end{aligned} \tag{3.12}$$

We consider two types of uniform partition in two dimensional space. There are uniform triangle mesh and uniform square mesh. Those meshes are demonstrated in Figure 2.1 and Figure 3.2, respectively. The special points which have the superconvergence property are the barycenters of each element. However, we also observe the superconvergence phenomenon at the center of the element face in uniform square mesh, while the convergence order is $m+2$.

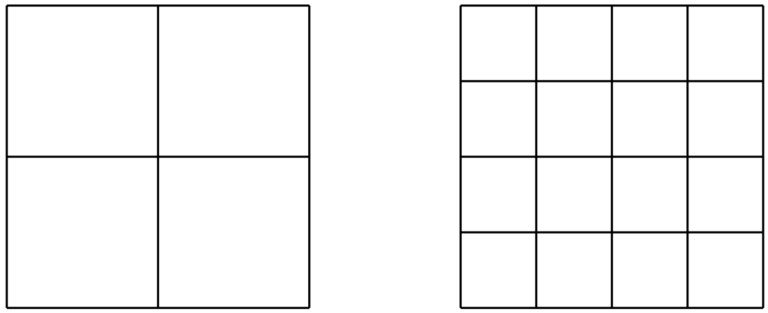

Figure 3.2. Uniform square mesh.

Proposition 3.2. *If the partition $\mathcal{T}_h$ are uniform distributed in two dimensional space, u and u_h are the solution in Theorem 3.4, and additionally $u \in H^{m+2}(\Omega)$, such that the superconvergence property with $m+2$ order at the barycenters of each elements are satisfied, i.e.*

$$\| u - \mathcal{R}u_h \|_h \leq Ch^{m+2} \, | \, u \, |_{H^{m+2}(\Omega)} . \tag{3.13}$$

Meanwhile, if the partition $\mathcal{T}_h$ is uniform square mesh, the superconvergence also can be observed at center of element faces.

$$\| u - \mathcal{R}u_h \|_h \leq Ch^{m+2} \, | \, u \, |_{H^{m+2}(\Omega)} . \tag{3.14}$$

The superconvergence results in three dimensional space do not coincide with the situation in two dimensional. We can not observe the superconvergence property at the barycenters of elements. The domain Ω is partitioned into uniform tetrahedron or hexahedron meshes which are shown in Figure3.3. The superconvergence property with $m+2$ order can be observed at the centers of each face of the elements.

Proposition 3.3. *If the partition $\mathcal{T}_h$ are uniformly distributed in three dimensional space, u and u_h are the solution in Theorem 3.4, and additionally $u \in H^{m+2}(\Omega)$, such that the superconvergence property with $m+2$ order at the center of each face of the elements are satisfied, i.e.*

$$\| u - \mathcal{R}u_h \|_h \leq Ch^{m+2} \, | \, u \, |_{H^{m+2}(\Omega)} . \tag{3.15}$$

4. Numerical Experiments

In this section, we present numerical results for the superconvergence property of the PRDG method. All the meshes are uniformly distributed as was presented. We first demonstrate the relation between the sparsity pattern of the resulting linear system and the size of the element patch. We employ the uniform tetrahedron mesh to partition the cubic domain with 3072 elements. The linear reconstruction is conducted with the patch size 7 and 16, and the quadratic reconstruction is conducted with the patch size being 16. Figure 4.1 shows the three sparsity patterns with different reconstruction and patch size.

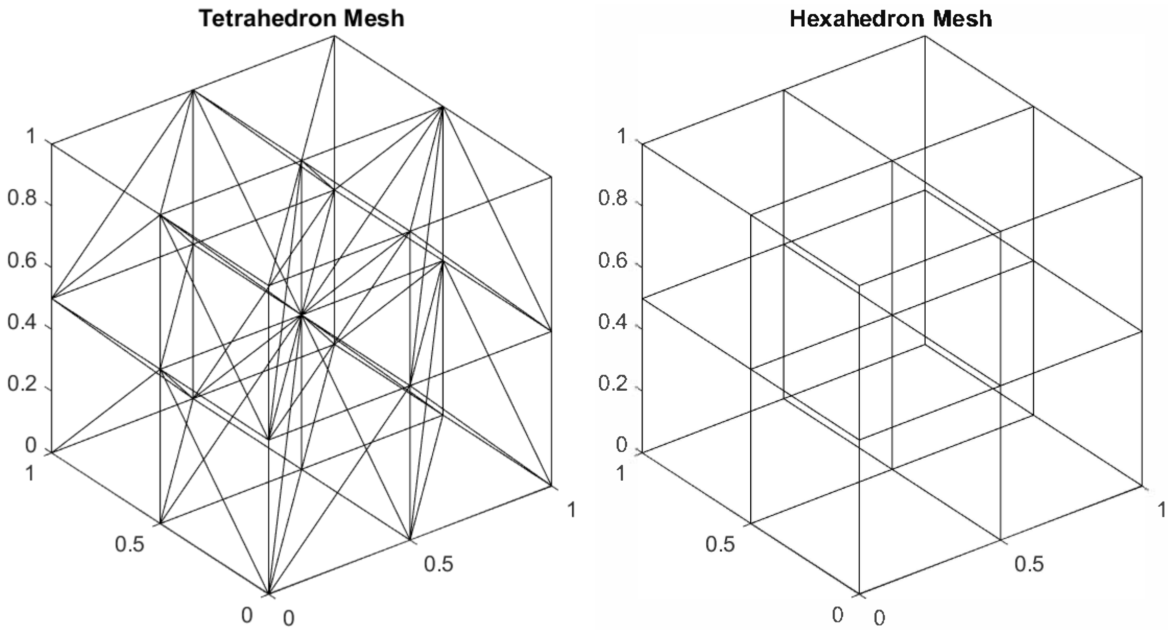

Figure 3.3. The uniform tetrahedron mesh (left)/ and the hexahedron mesh(right).

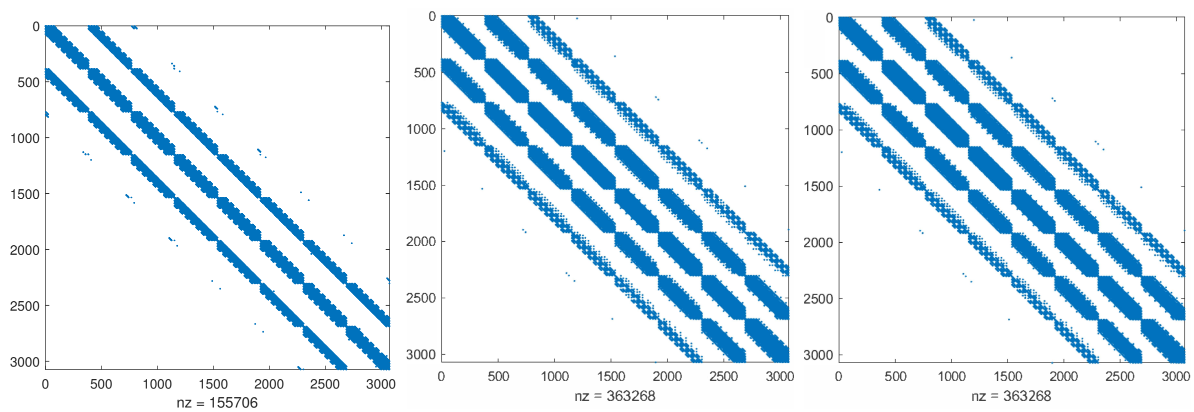

Figure 4.1. The sparsity patterns of the linear systems: The linear reconstruction with 7 patch size(left)/The linear reconstruction with 16 patch size(middle)/The quadratic reconstruction with 16 patch size(right)

Firstly, we can observe that the size of all the linear system is 3072×3072 , regardless of the reconstruction. Then compare the left two subfigures, which are the linear reconstruction with different patch sizes. The sparsity pattern changes when the element patch and the number of nonzero elements increases. However, the right two subfigures demonstrate the linear reconstruction and the quadratic reconstruction with the same patch size. The sparsity patterns and the number of nonzero terms coincide with each other. Generally, the sparsity of the resulting linear system is mainly determined by the size of the element patch, and when the reconstruction order increases, the larger element patch is demanded, which will lead the sparsity to get slightly worse. In the numerical

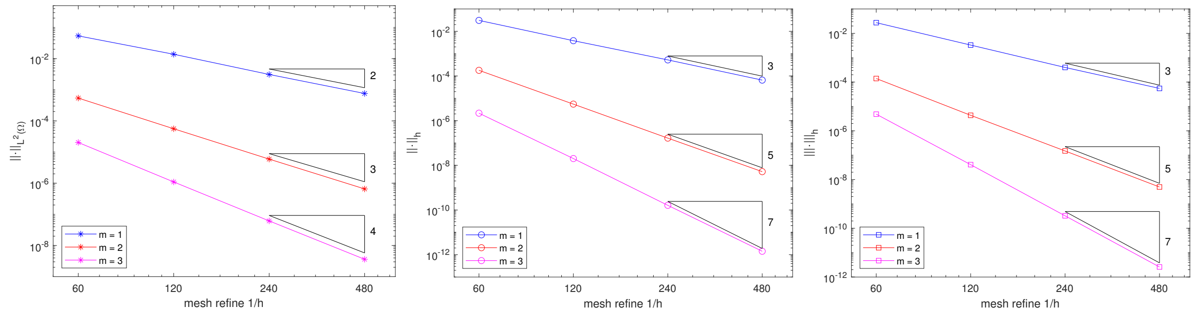

Figure 4.2. The convergence order of $\|u - \mathcal{R}u_h\|_{L^2(\Omega)}$(left)/$\| u - \mathcal{R}u_h \|_h$(middle)/$\|| u - \mathcal{R}u_h \||_h$(right) with different order m in 1D.

m	$\| u - \mathcal{R}u_h \|_{L^2(\Omega)}$ error order	$\| u - \mathcal{R}u_h \|_h$ error order	$\|\| u - \mathcal{R}u_h \|\|_h$ error order
1	1.9603	2.9605	3.0536
2	3.2727	5.0225	5.0127
3	4.2114	6.8449	6.8847

Table 4.1. The convergence order of the different norms in 1D.

m	$\| u - \mathcal{R}u_h \|_{L^2(\Omega)}$ error order	$\| u - \mathcal{R}u_h \|_h$ error order
1	1.9841	3.1221
2	3.3599	4.2205
3	4.0463	4.9108
4	5.2886	5.8989

Table 4.2. The convergence rate of different norms in 2D triangle mesh.

experiments, we usually take the element patch sightly larger than the DOFs of high order polynomial reconstruction needs.

4.1. **One dimensional results.** In one dimensional occasion, the exact solution is taken as $u(x) = \sin(2\pi x)$, the corresponding right hand side is $f = 4\pi^2 \sin(2\pi x)$ and the Dirichlet boundary condition $u(0) = u(1) = 0$ is weakly satisfied.

In Figure 4.2 and Table 4.1, we present the convergence rate for this Poisson equation which is solved by the PRDG method with different norms. At the mesh points and the barycenters of the grids, we obtain $2m + 1^{\text{th}}$ order convergence rate while the L^2 norm error is $m + 1$. The results agree with the Proposition 3.1.

4.2. **Two dimensional results.** We consider the Poisson equation with the Dirichlet boundary in the square domain. The exact solution is $u(x) = \sin(2\pi x)\sin(2\pi y)$, and the superconvergence property is slightly different with the one dimensional case. Figure 4.3 and Table 4.2 shows the numerical results in uniform triangle meshes. The superconvergence appears at the barycenters of each element with $m + 2$ order. However, the convergence rate at the centers of each element faces is consistent with the L^2 norm error.

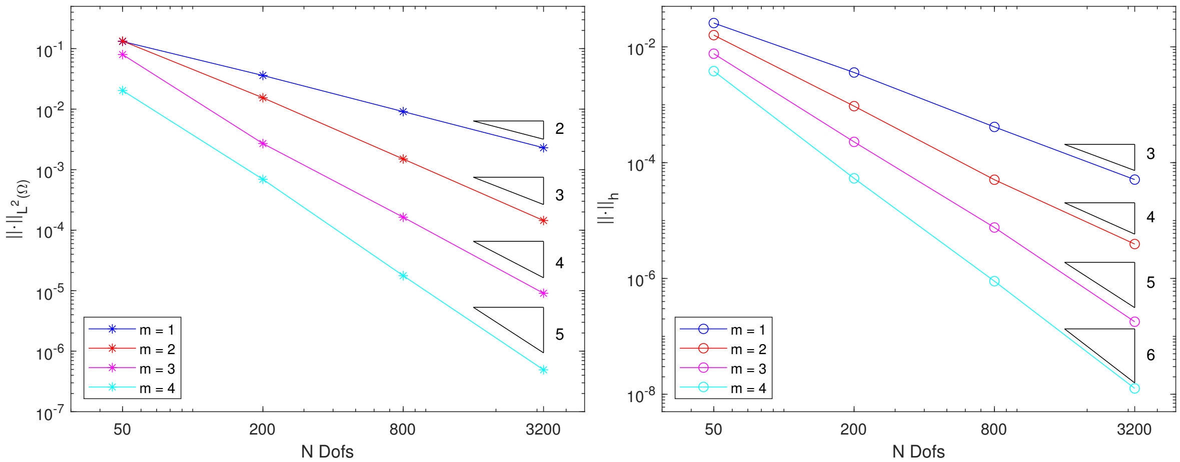

Figure 4.3. The convergence order of $\|u - \mathcal{R}u_h\|_{L^2(\Omega)}$(left)/$\| u - \mathcal{R}u_h \|_h$(right) with different order m in 2D triangle mesh.

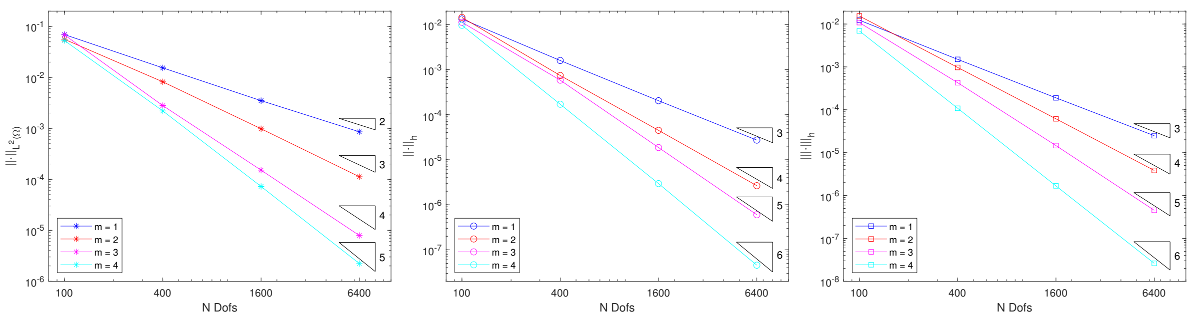

Figure 4.4. The convergence order of $\|u - \mathcal{R}u_h\|_{L^2(\Omega)}$(left)/$\| u - \mathcal{R}u_h \|_h$(middle))/$\|| u - \mathcal{R}u_h \||_h$(right) with different order m in in 2d square mesh.

m	$\| u - \mathcal{R}u_h \|_{L^2(\Omega)}$ error order	$\| u - \mathcal{R}u_h \|_h$ error order	$\|\| u - \mathcal{R}u_h \|\|_h$ error order
1	2.1375	2.9830	2.9666
2	3.0613	3.9890	3.9863
3	4.2076	4.8476	4.9693
4	4.9222	6.0021	6.0122

Table 4.3. The convergence rate of different norms in 2D square mesh

Figure 4.4 and Table 4.3 present the square meshes numerical results. The superconvergence property can be achieved at the grid points and the element face centers at the same time. The convergence rate is $m + 2$ which is also coincides with Proposition 3.2.

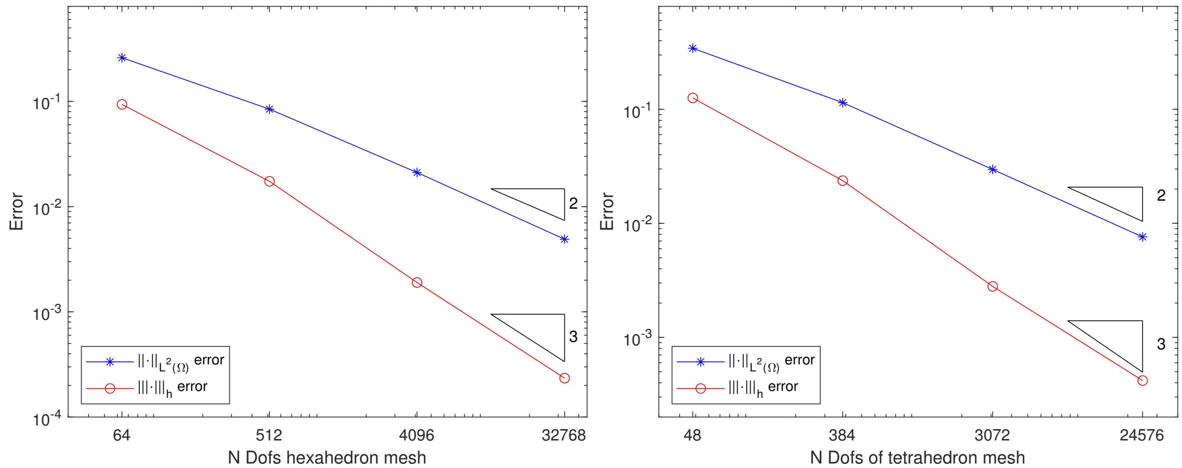

Figure 4.5. The convergence order of hexahedron mesh(left)/tetrahedron mesh(right) of linear reconstruction with different norms in 3D.

Mesh type	$\| u - \mathcal{R}u_h \|_{L^2(\Omega)}$ error order	$\|\| u - \mathcal{R}u_h \|\|_h$ error order
Tetrahedron	1.9468	3.0814
Hexahedron	2.1064	3.0191

Table 4.4. The convergence order of linear reconstruction with different norms in 3D mesh

4.3. **Three dimensional results.** Finally, we present a three dimensional example. The Poisson equation with exact solution $u = \sin(2\pi x)\sin(2\pi y)\sin(2\pi z)$ is considered. Figure 4.5 and Table 4.4 shows the linear reconstruction numerical results. The superconvergence only can be achieved at the centers of element faces. The convergence rate is $m + 2$ which is also meet with Proposition 3.3 well.

5. Conclusions

The superconvergence property of the PRDG method for elliptic problems is investigated numerically. Details of numerical implementations are presented and the sparsity patterns of resulting linear systems are remonstrated. The superconvergence results are achieved at the face centers or the barycenters of the element in function values with the uniform partitions.

Acknowledgment

The research is supported by the National Natural Science Foundation of China (Grant No. 11671312, 91630313), the Natural Science Foundation of Hubei Province (Grant No. 2019CFA007), and China Postdoctoral Science Foundation (Grant No. 2019M660558). The numerical calculations have been done on the supercomputing system in the Supercomputing Center of Wuhan University.

References

[1] M. Ainsworth and J. T. Oden. *A posteriori error estimation in finite element analysis*. Pure and Applied Mathematics (New York). Wiley-Interscience [John Wiley & Sons], New York, 2000.

[2] D. N. Arnold. An interior penalty finite element method with discontinuous elements. *SIAM J. Numer. Anal.*, 19(4):742–760, 1982.

[3] M. Bakker. One-dimensional Galerkin methods and superconvergence at interior nodal points. *SIAM J. Numer. Anal.*, 21(1):101–110, 1984.

[4] W. Cao, C.-W. Shu, Y. Yang, and Z. Zhang. Superconvergence of discontinuous Galerkin methods for two-dimensional hyperbolic equations. *SIAM J. Numer. Anal.*, 53(4):1651–1671, 2015.

[5] P. Castillo. A superconvergence result for discontinuous Galerkin methods applied to elliptic problems. *Comput. Methods Appl. Mech. Engrg.*, 192(41-42):4675–4685, Castillo.

[6] B. Cockburn, J. Guzmán, and H. Wang. Superconvergent discontinuous Galerkin methods for second-order elliptic problems. *Math. Comp.*, 78(265):1–24, 2009.

[7] B. Cockburn, G. Kanschat, I. Perugia, and D. Schötzau. Superconvergence of the local discontinuous Galerkin method for elliptic problems on Cartesian grids. *SIAM J. Numer. Anal.*, 39(1):264–285, 2001.

[8] B. Cockburn, W. Qiu, and K. Shi. Conditions for superconvergence of HDG methods for second-order elliptic problems. *Math. Comp.*, 81(279):1327–1353, 2012.

[9] B. Cockburn, W. Qiu, and K. Shi. Superconvergent HDG methods on isoparametric elements for second-order elliptic problems. *SIAM J. Numer. Anal.*, 50(3):1417–1432, 2012.

[10] J. Douglas, Jr. and T. Dupont. Some superconvergence results for Galerkin methods for the approximate solution of two-point boundary problems. In *Topics in numerical analysis (Proc. Roy. Irish Acad. Conf., University Coll., Dublin, 1972)*, pages 89–92, 1973.

[11] R. Li, P. Ming, Z. Sun, F. Yang, and Z. Yang. A discontinuous Galerkin method by patch reconstruction for biharmonic problem. *J. Comput. Math.*, 37(4):563–580, 2019.

[12] R. Li, P. Ming, Z. Sun, and Z. Yang. An arbitrary-order discontinuous Galerkin method with one unknown per element. *J. Sci. Comput.*, 80(1):268–288, 2019.

[13] R. Li, Z. Sun, F. Yang, and Z. Yang. A finite element method by patch reconstruction for the Stokes problem using mixed formulations. *J. Comput. Appl. Math.*, 353:1–20, 2019.

[14] R. Li, Z. Sun, and Z. Yang. A discontinuous Galerkin method for Stokes equation by divergence-free patch reconstruction. *Numer. Methods Partial Differential Equations*, 36(4):756–771, 2020.

[15] R. Li, Z. Y. Sun, and F. Y. Yang. Solving eigenvalue problems in a discontinuous approximate space by patch reconstruction. *SIAM J. Sci. Comput.*, 41(5):A3381–A3400, 2019.

[16] R. Li and F. Yang. A least squares method for linear elasticity using a patch reconstructed space. *Comput. Methods Appl. Mech. Engrg.*, 58(1):353–374, 2020.

[17] R. Li and F. Yang. A sequential least squares method for Poisson equation using a patch reconstructed space. *SIAM J. Numer. Anal.*, 58(1):353–374, 2020.

[18] Z. Sun, J. Liu, and P. Wang. A discontinuous Galerkin method by patch reconstruction for convection-diffusion problems. *Adv. Appl. Math. Mech.*, 12(3):729–747, 2020.

[19] B. van Leer. Towards the ultimate conservative difference scheme. V. A second-order sequel to Godunov's method [J. Comput. Phys. **32** (1979), no. 1, 101–136]. volume 135, pages 227–248. 1997. With an introduction by Ch. Hirsch, Commemoration of the 30th anniversary {of J. Comput. Phys.}.

[20] L. B. Wahlbin. *Superconvergence in Galerkin finite element methods*, volume 1605 of *Lecture Notes in Mathematics*. Springer-Verlag, Berlin, 1995.

[21] J. Wang and X. Ye. A weak Galerkin finite element method for second-order elliptic problems. *J. Comput. Appl. Math.*, 241:103–115, 2013.

[22] R. Wang, R. Zhang, X. Zhang, and Z. Zhang. Supercloseness analysis and polynomial preserving recovery for a class of weak Galerkin methods. *Numer. Methods Partial Differential Equations*, 34(1):317–335, 2018.

[23] Y. Yang and C.-W. Shu. Analysis of optimal superconvergence of discontinuous Galerkin method for linear hyperbolic equations. *SIAM J. Numer. Anal.*, 50(6):3110–3133, 2012.

[24] O. C. Zienkiewicz and J. Z. Zhu. The superconvergent patch recovery and a posteriori error estimates. I. The recovery technique. *Internat. J. Numer. Methods Engrg.*, 33(7):1331–1364, 1992.

School of Mathematics and Statistics, Wuhan University, Wuhan 430072, P.R. China
Email address: zexuanliu@whu.edu.cn

Institute of Applied Physics and Computational Mathematics, Beijing 100094, P.R. China
Email address: zysun.math@gmail.com

School of Mathematics and Statistics & Computational Science Hubei Key Laboratory, Wuhan University, Wuhan 430072, P.R. China
Email address: zjyang.math@whu.edu.cn